Water Resources Research

RESEARCH ARTICLE
10.1029/2025WR041632

Two Centuries of Streamflow Behavior Inferred From Freshwater Pearl Mussel Shell $\delta^{18}O$ in Northern Sweden

Christoph J. Gey[1], Guilhem Türk[2,3], Laurent Pfister[2,3], Hjalmar Laudon[4], Frankie Thielen[5], and Bernd R. Schöne[1]

[1]Institute of Geosciences, University of Mainz, Mainz, Germany, [2]Catchment and eco-hydrology group/Environmental sensing and modelling unit, Luxembourg Institute of Science and Technology, Belvaux, Luxembourg, [3]Faculty of Science, Technology and Medicine, University of Luxembourg, Technology and Medicine, Esch-sur-Alzette, Luxembourg, [4]Department of Forest Ecology and Management, Swedish University of Agricultural Sciences, Umeå, Sweden, [5]natur&ëmwelt, Fondation Hëllef Fir D'Natur, Marnach, Luxembourg

Christoph J. Gey and Guilhem Türk share first authorship.

Christoph J. Gey and Guilhem Türk contributed equally to this work.

Abstract Global warming alters snowmelt timing and soil frost cycles, impacting storage-discharge dynamics of subarctic catchments. Assessing how these changes affect streamflow requires quantifying the relative contribution of winter versus summer precipitation. While this can be achieved based on oxygen isotope data ($\delta^{18}O$) in precipitation and streamwater, the full potential of this approach is hindered by short and truncated time-series. Here we overcome this limitation by combining modeled precipitation $\delta^{18}O$ time-series with streamwater $\delta^{18}O$ data from freshwater pearl mussel shells. Based on more than 2,700 shell-derived streamwater $\delta^{18}O$ values reconstructed from four Northern Swedish catchments we estimated contributions of precipitation to streamflow since 1836. The reconstructed $\delta^{18}O$ streamwater records, which typically capture summer low-flow conditions during the growing season of the mussels, showed pronounced differences between catchments. In a monitored reference catchment, a negative correlation between baseflow and $\delta^{18}O$-derived contributions of summer precipitation suggests that these differences reflect catchment-specific variations in baseflow during low-flow conditions. These variations in seasonal precipitation contributions to streamflow were linked to physiographic catchment characteristics, which also affected long-term summer low flow conditions. Reconstructions based on bivalve shells therefore provide insights into how landscape features (e.g., catchment size, soil conductivity, lakes) influence water transit times and delay the release of winter precipitation across catchments over centuries. With this transferable and scalable approach, isotope data sets can be extended into pre-instrumental times, supporting adaptive water-resource management in data-scarce regions.

Plain Language Summary In subarctic regions, climate change is causing snow to melt earlier in the year which shifts the timing of the spring flood. These changes may reduce water availability in summer and make streams more vulnerable to drought. To assess this risk, it is important to understand how much of the streamflow comes from winter snow versus summer rain. Oxygen isotopes in precipitation carry seasonal signals that can be detected in streamwater. However, direct measurements are often short-term and limited to a few research catchments. We addressed this by combining model-based isotope data with oxygen isotope records preserved in the shells of long-lived freshwater mussels. By analyzing over 2,700 shell samples from northern Sweden, we estimated how much summer and winter precipitation contributed to streamflow in four rivers since 1836. We found that landscapes with lakes and peatlands helped to stabilize flow during dry summers. This method can be applied worldwide to improve water management, especially in regions without long-term monitoring data.

Key Points:

- Centuries of hydrological information are archived in the oxygen isotopes of the shells of long-lived freshwater mussels
- Combining shell and modeled precipitation oxygen isotope data reveals subarctic catchment responses to climate change
- The oxygen isotope-based seasonal origin index is a robust metric to assess summer drought vulnerability in boreal streams

Supporting Information:

Supporting Information may be found in the online version of this article.

Correspondence to:

C. J. Gey and G. Türk,
christoph.gey@uni-mainz.de;
guilhem.turk@hotmail.com

Citation:

Gey, C. J., Türk, G., Pfister, L., Laudon, H., Thielen, F., & Schöne, B. R. (2025). Two centuries of streamflow behavior inferred from freshwater pearl mussel shell $\delta^{18}O$ in northern Sweden. *Water Resources Research*, *61*, e2025WR041632. https://doi.org/10.1029/2025WR041632

Received 14 JUL 2025
Accepted 2 DEC 2025

Author Contributions:

Conceptualization: Laurent Pfister, Bernd R. Schöne
Data curation: Christoph J. Gey, Guilhem Türk
Formal analysis: Christoph J. Gey, Guilhem Türk
Funding acquisition: Laurent Pfister, Bernd R. Schöne

1. Introduction

High latitude rivers are very sensitive to climate change. With the climate of subarctic regions warming at a rate that exceeds the global average (Intergovernmental Panel On Climate Change (IPCC), 2023: CCP6), regional snowmelt-driven runoff regimes are increasingly affected by changes in freeze-thaw dynamics. These shifts do not only influence the timing and magnitude of spring floods (Liu et al., 2005; Teutschbein et al., 2015; Zhang et al., 2001), they also impact surface-groundwater interactions by changing soil conductivity across freeze and thaw periods (Jutebring Sterte et al., 2018; Laudon et al., 2007). The combination of these shifts in hydrological processes with changes in precipitation (e.g., seasonal distribution, intensity), ultimately modifies the fundamental hydrological catchment functions of water collection, storage, mixing and release.

Investigation: Christoph J. Gey, Guilhem Türk
Methodology: Christoph J. Gey, Guilhem Türk, Frankie Thielen
Project administration: Laurent Pfister, Bernd R. Schöne
Resources: Hjalmar Laudon, Frankie Thielen
Supervision: Laurent Pfister, Bernd R. Schöne
Validation: Laurent Pfister, Hjalmar Laudon, Bernd R. Schöne
Visualization: Christoph J. Gey, Guilhem Türk
Writing – original draft: Christoph J. Gey, Guilhem Türk
Writing – review & editing: Laurent Pfister, Hjalmar Laudon, Frankie Thielen, Bernd R. Schöne

Preserving ecosystem services in boreal regions is a pressing challenge. In such landscapes peatbogs are pivotal for water, nutrient and carbon fluxes (Karimi et al., 2024). For northern Sweden, multiple studies have reported a tendency toward a wetter climate, associated with increasing streamflow over the twentieth century (Lindström & Bergström, 2004; Teutschbein et al., 2022; Wilson et al., 2010). However, projections also suggest that rising air temperature, increased evapotranspiration, reduced snow cover and earlier, attenuated spring floods may lead to a decline in seasonal discharge (Arheimer & Lindström, 2015). Furthermore, all studies consistently report large catchment-specific variations as well as strong seasonal differences.

Predicting future changes in streamflow remains challenging, essentially due to the complex interplay of factors influencing hydrological processes. Bedrock geology (Gabrielli & McDonnell, 2020; Katsuyama et al., 2010; Pfister et al., 2017), soils (Devito et al., 2017; Karlsen et al., 2016; Ploum et al., 2019), vegetation (Alavi et al., 2001; Grelle et al., 1997; Laudon et al., 2007), land-use (Meriö et al., 2019; Teutschbein et al., 2015, 2018) and human regulations (Arheimer et al., 2017) significantly affect fundamental hydrological catchment functions. Therefore, simple (conceptual) water balance models often fail in capturing regional drought or flood dynamics (Arheimer et al., 2017; Goodbrand et al., 2019; Rouse et al., 1997). Catchment functions are notoriously non-stationary and non-linear, and little is currently known about the processes that drive this variability (Benettin et al., 2022; Kirchner, 2006). One of the largest knowledge gaps remains how catchments release water from the subsurface, which prevents projections into future streamflow behavior (Fan et al., 2019). In catchments located at higher altitudes and/or latitudes, the catchment water storage capacity and transit times are closely related to freeze-thaw cycles and freezing depths. The freeze-thaw cycles are expected to change under a warming climate and thus believed to impact storage-discharge relationships in boreal streams (Ala-Aho et al., 2021; Ploum et al., 2019; Rouse et al., 1997).

The disruption of the freeze-thaw cycle and the redistribution of the annual streamflow will likely not only affect spring floods, but also exacerbate drought conditions. Large amounts of precipitation falling in one season may—if temporarily stored in the catchment—contribute to streamflow in subsequent seasons (Allen et al., 2019). Despite higher streamflow volumes with increasing precipitation, higher rain-to-snow ratios and an earlier onset of snowmelt ultimately mean less storage in the catchments in spring and early summer (Teutschbein et al., 2015). This could be problematic for low-flow conditions in summer, eventually threatening minimal environmental flows required to support the ecological integrity of the streams. Thus, analyzing the historical seasonal water budgets and long-term storage-discharge relationships is essential to assess the vulnerability of catchments to droughts.

To track the variability of the seasonal partitioning of precipitation into streamflow, Allen et al. (2019) introduced the Seasonal Origin Index (SOI). The SOI relies on seasonal patterns in oxygen isotope values of precipitation ($\delta^{18}O_{precipitation}$), particularly pronounced in northern regions where winter ($\delta^{18}O_{Pwinter}$) and summer ($\delta^{18}O_{Psummer}$) signatures exhibit strong contrasts. By comparing the streamwater oxygen isotope composition ($\delta^{18}O_{streamwater}$) with the corresponding seasonal $\delta^{18}O$ fingerprint of precipitation, the SOI can be used to quantify the relative contribution to streamflow of winter versus summer precipitation. The determination of the SOI requires seasonally resolved records of $\delta^{18}O$ in both precipitation and streamwater. However, the scarcity of historic precipitation and streamwater $\delta^{18}O$ records (covering more than a decade) limits the potential of isotope-based approaches. While the Global Network of Isotopes in Precipitation (GNIP) data are spatially limited and only extend back to the early 1960s for individual sites, recent advances in numerical modeling and machine learning have improved the ability to estimate precipitation $\delta^{18}O$ values across Europe, dating back to the early twentieth century (Nelson et al., 2021; Türk et al., 2025). To address the limited availability of $\delta^{18}O_{streamwater}$ records, sclerochronological studies have leveraged the potential of freshwater mollusk shells as natural archives of past streamwater isotope compositions (Kelemen et al., 2017; Pfister et al., 2018, 2019; Schöne et al., 2020; Versteegh et al., 2010). During their growth, mollusks encode the $\delta^{18}O$ values of the surrounding water in the mineral fraction ($CaCO_3$) of their shells. These data can be chronologically attributed by analyzing shell growth patterns. The rate at which the shells grow is largely controlled by water temperature and food availability and encoded in the width of growth increments—similar to tree rings.

A global assessment of shell isotope data from freshwater bivalves and snails showed that their $\delta^{18}O$ signatures can explain 95% in the variation in streamwater $\delta^{18}O$ (Pfister et al., 2019). For northern Europe, the most promising $\delta^{18}O_{streamwater}$ archive are the shells of the freshwater pearl mussel, *Margaritifera margaritifera*. This species biomineralizes the outer portion of the outer shell layer (oOSL, prismatic ultrastructure, aragonite) close

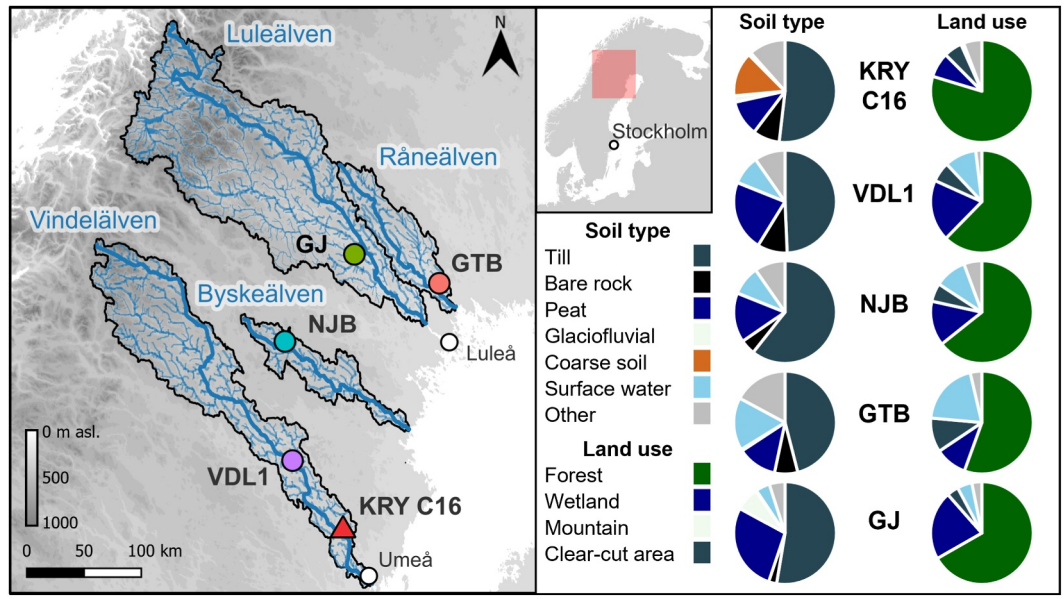

Figure 1. Map showing the extents of the catchments of the primary streams and the bivalve collection sites in northern Sweden. KRY C16 (red triangle) serves as a reference site with in situ $\delta^{18}O_{streamwater}$ data, while the other locations (VDL1, NJB, GTB, GJ) are the shell collection sites. The pie charts illustrate the distribution of soil types and land use categories for the catchments of the four sampling localities. Digital elevation model of the basemap, watersheds and river network are based on Lehner et al. (2008). Data available at https://www.hydrosheds.org (last access: 12 February 2025).

to thermodynamic equilibrium with the ambient water, resulting in a high reproducibility of reconstructed water $\delta^{18}O$ values among specimens from the same stream (Gey et al., 2024; Pfister et al., 2018; Schöne et al., 2020). Particularly in cold streams, *Margaritifera margaritifera* can reach exceptional lifespans of more than 200 years (Mutvei & Westermark, 2001). This longevity has enabled uninterrupted, high-resolution, multi-century $\delta^{18}O_{streamwater}$ reconstructions from single specimens (Schöne et al., 2020).

To answer the pressing questions of long-term responses of streamflow to a changing climate in northern latitude catchments and related streamflow resilience to climate change, we formulate three complementary hypotheses:

1. A centennial chronology of seasonal origins of streamwater (SOI) can be reliably reconstructed from model-derived precipitation $\delta^{18}O$ data and sclerochronology-based streamwater $\delta^{18}O$ time-series.
2. Reconstructed SOI are a robust metric for assessing long-term dynamics in summer low-flow conditions in boreal landscapes.
3. SOI chronologies are influenced by local physiographic characteristics and serve as a proxy for assessing their effect on the response of streamflow to changes in the hydrological cycle.

To test these hypotheses, we rely on reconstructed pre-instrumental $\delta^{18}O$ series (a) in precipitation from existing models based on atmospheric circulation patterns (Nelson et al., 2021; Türk et al., 2025) and (b) in streamwater from 1836 to 2023 CE using 13 *Margaritifera margaritifera* shells from four catchments in northern Sweden. We use the reconstructed $\delta^{18}O$ time-series to derive SOI chronologies representative of the growing season of the mussel (i.e., June to August) and compare them against a 12-year in situ $\delta^{18}O$ record from a nearby catchment, including both precipitation and streamflow data. By estimating the SOI over almost two centuries, we explore how climate change has affected and may continue to impact catchment hydrology in boreal regions.

2. Material and Methods

2.1. Shell Sampling Locations and Study Sites

In fall 2023, 15 adult freshwater pearl mussels (*Margaritifera margaritifera*) were collected alive from a third order tributary (VDL1) of the Vindelälven in Västerbotten County, northern Sweden (Figure 1; Table 1). This collection had been authorized by the local county administration (Länsstyrelsen Västerbotten; Permit No. 623-7313-2023). Three shells were used for isotope analysis, yielding 1,654 $\delta^{18}O_{shell}$ datapoints, covering the time interval of

Table 1
Location and Attributes of Margaritifera margaritifera Shells Used in the Present Study

Stream	Stream ID	Catchment area (m^2)	Elevation (m a.s.l.)	Specimen ID	Coordinates	Age[b] (years)	Lifespan (year CE)	N
3rd order tributary of Vindelälven[a]	VDL1	79.5	ca. 230	2023-VDL1-A5	64°45'00.00"N, 019°00'00.00"E	64	1960–2023	497
				2023-VDL1-A7		213	1811–2023	442
				2023-VDL1-A12		147	1877–2023	715
Nuortejaur-bäcken	NJB	38.1	ca. 400	ED-NJB-A2R	65°42'13.22" N, 019°02'31.01" E	48	1946–1993	78
				ED-NJB-A3R		24	1970–1993	50
				ED-NJB-A4R		27	1967–1993	154
				ED-NJB-A6R		22	1972–1993	175
Grundträsktjärn-bäcken	GTB	8.9	ca. 90	ED-GTB-A1R	66°02'59.98" N, 022°05′02.25" E	51	1943–1993	368
				ED-GTB-A2R		51	1943–1993	315
Görjeån	GJ	215.8	ca. 200	ED-GJ-A1L	66°20'30.77" N, 020°30′15.02" E	82	1916–1997	56
				ED-GJ-A2R		80	1918–1997	76
				ED-GJ-A3L		123	1875–1997	110
				ED-GJ-D5L		181	1819–1999	169

Note. Specimens from NJB, GTB and GJ were previously analyzed by Schöne et al. (2020). The suffix in the specimen ID indicates if the bivalve was collected alive (*A*) or found dead (*D*). The *N* column contains the number of $\delta^{18}O_{shell}$ measurements obtained from each bivalve. [a]To protect the population, the tributary of the latest sampling site VDL1 is not named, and coordinates are rounded. [b]Minimum estimated life span, erosion in the umbonal shell portion obscures approx. 10 additional years.

1811–2023. The remaining 12 shells were used for annual growth pattern analysis to establish an accurate age model via crossdating. To extent the data set, we used previously published shell-based $\delta^{18}O_{streamwater}$ reconstructions by Schöne et al. (2020) from specimens collected between 1993 and 1999 in Norrbotten County, ca. 300 km north of the VDL1 site. This additional data set includes four individuals from Nuortejaurbäcken (NJB, tributary of the Byskeälven), two from Grundträsktjärnbäcken (GTB, tributary of the Råneälven) and four from the Görjeån River (GJ, tributary of the Luleälven) and is based on 1,551 $\delta^{18}O_{shell}$ datapoints, covering the period 1819 to 1998.

Isotope data from the experimental Krycklan Catchment Study (KCS), a facility known for its extensive research on boreal systems (Laudon et al., 2021) and another tributary of the Vindelälven located about 70 km downstream from VDL1, was used as a reference in this study. Here, we use a subset of sub-monthly in situ precipitation and streamwater $\delta^{18}O$ measurements spanning from January 2011 to December 2023 (2016–2022 for sub-monthly measurements in precipitation). Sampling was typically conducted two to four times per week, depending on precipitation events and logistical constraints (due to extremely cold temperatures in winter). These data are openly available for catchment 16 (KRY C16) in the data catalog of the Swedish Infrastructure for Ecosystem Science (SITES) (available at https://data.fieldsites.se/portal/; last access: 15 June 2024). Although the catchment is currently not hosting any known freshwater pearl mussels, it still provides a valuable reference for the isotope composition of precipitation and streamflow in the region and serves as a benchmark for the reconstructed SOI time-series using shell-derived $\delta^{18}O_{streamwater}$ chronologies. In addition to the SOI, streamflow metrics were also calculated at KRY C16 to assess and establish relationships between the seasonal composition of streamwater and the streamflow response at the catchment scale.

2.2. Catchment Characteristics

The freshwater pearl mussels stem from four catchments of different sizes: GTB (8.9 km^2), NJB (38.1 km^2), VDL1 (79.5 km^2) and GJ (215.8 km^2), all underlain by orthogneiss and granodiorite bedrock. Despite their varying sizes, these catchments share characteristics representative of the boreal landscape (Figure 1). All are predominantly forested, with a significant presence of unsorted till (glacial debris) soils, peat soils and open water bodies. Till soils dominate across all sites, covering about 55% in GTB, VDL1 and GJ, and 66% in NJB. Peat soils are most extensive in GJ (29%) and VDL1 (25%), and somewhat lower in NJB (17%) and GTB (15%). Open water varies considerably, with GTB having the highest proportion (20%), followed by VDL1 and NJB (10%), while GJ

has only 5%. Forest cover is relatively consistent (56%–67%): GTB and GJ are dominated by mixed birch forest, whereas NJB and VDL1 are primarily coniferous.

The Krycklan reference catchment 16 (KRY C16) has a similar overall land use cover, with 52% till and 11% peat soils. It contains very little open water (<1%) but has the highest forest coverage, predominantly coniferous. All catchments, including the reference and the mussel sampling sites, are free from urban areas and significant agricultural land.

2.3. Base Flow Calculations at the Reference Site for Proof-of-Concept

Baseflow is a common metric used to assess groundwater contributions to total streamflow in gauged catchments. Here, we use it at the KRY C16 reference site to demonstrate links between the baseflow and the seasonal origin of streamflow, as a proof-of-concept for the interpretation of historic shell-based SOI signals. Streamflow data was also obtained from the data catalog of the Swedish Infrastructure for Ecosystem Science (SITES) (available at https://data.fieldsites.se/portal/; last access: 15 June 2024). It was available at daily resolution for the years 2016–2022, but with interruptions in the winter period due to ice cover. The baseflow is obtained through hydrograph separation, which provides information on recent precipitation inputs and slow releases of water stored in the catchment, or fast and slow components of the streamflow response. Note that the origins of streamflow and the speed of streamflow processes are different concepts and depend on the methods used to perform the hydrograph separation (e.g., tracer-based vs. graphically-based). In this study, we used the Lyne and Hollick (1979) filter, a recursive digital filter for signal analysis (Nathan & McMahon, 1990), as used in Ladson et al. (2013). The latter proposed a standard procedure to obtain reproducible base flow estimates. The underlying equation can be written as follows:

$$Q_f(t) = \begin{cases} \alpha\, Q_f(t-1) + \dfrac{1+\alpha}{2}\,(Q(t) - Q(t-1)), & Q_f(t) > 0 \\ 0, & Q_f(t) < 0 \end{cases} \quad (1)$$

where $Q(t)$ is the streamflow at a time step t - here the daily specific discharge, $Q(t–1)$ is the streamflow at the previous time step, $Q_f(t)$ is the fast flow component of the total streamflow applying the filter, and $Q_f(t–1)$ is the fast flow component at the previous time step. The parameter α defines the degree of separation between low and high frequency signals and thus the shape of the base flow line. By filtering out the high-frequency spectrum of the hydrograph, this method merely approximates the slower contributions of groundwater to streamflow. Still, the filter is a good first approach, especially in combination with tracer data, and has already been used in this regard for the Krycklan catchment in previous studies (Teutschbein et al., 2015).

With the estimate of the fast flow component, the base flow $Q_b(t)$ at time step t can be defined as:

$$Q_b(t) = Q(t) - Q_f(t) \quad (2)$$

For the reproducibility of the results following Ladson et al. (2013), only sequences of continuous non-missing streamflow values were considered. This was particularly relevant for KRY C16, containing missing values during the winter period. A threshold of 100 consecutive observations was set for the selection of the sequences. The 90 first and 90 last observations were reflected as "warm-up" intervals at the beginning of these sequences. These values were included in the calculations but excluded from the results to avoid boundary-condition issues. Three passes of the filter were applied to the streamflow time-series, following a forward, backward and forward order, with the α parameter set to 0.98.

The base flow index (BFI) at a time step t is simply defined as the ratio of base flow to the total flow:

$$\mathrm{BFI}(t) = \frac{Q_b(t)}{Q(t)} \quad (3)$$

Over the entire time-series (including all periods when data was available), the BFI is defined as the sum of all base flow divided by the sum of all total flow:

$$\mathrm{BFI} = \frac{\sum_{t=1}^{N} Q_b(t)}{\sum_{t=1}^{N} Q(t)} \quad (4)$$

2.4. The Seasonal Origin Index (SOI)

The SOI quantifies the relative contribution of different seasonal precipitation sources to streamwater on a scale from −1 to +1 (Allen et al., 2019). An SOI value of −1 would indicate that 100% of the streamflow at the time of measurement consists of winter precipitation, while an SOI value of +1 indicates that 100% consists of summer precipitation. Values between −1 and +1 represent mixtures of these seasonal endmembers. The calculation of the SOI requires the following input variables: δ_P as the mean annual $\delta^{18}O_{precipitation}$; $\delta_{Psummer}$ and $\delta_{Pwinter}$ as seasonal inputs of $\delta^{18}O_{precipitation}$ and δ_Q as the $\delta^{18}O_{streamwater}$ at the time of sampling.

$$\mathrm{SOI} = \begin{cases} \dfrac{\delta_Q - \delta_P}{\delta_{Psummer} - \delta_P}, \text{if } \delta_Q > \delta_P \\ \dfrac{\delta_Q - \delta_P}{\delta_P - \delta_{Pwinter}}, \text{if } \delta_Q < \delta_P \end{cases} \quad (5)$$

To calculate the SOI, $\delta^{18}O_{streamwater}$ data can directly be used in Equation 5 to produce SOI time-series reflecting seasonal changes of the streamwater origin. Alternatively, the mean of all $\delta^{18}O_{streamwater}$ values can be used to assess overall contributions of winter and summer precipitation to streamwater. In this study, shell-based $\delta^{18}O_{streamwater}$ values reflect streamwater conditions during the growing season of the bivalves (typically June to August), that is, primarily under summer baseflow conditions.

The amplitude of seasonal $\delta^{18}O_{precipitation}$ is defined as the range between the maximum ($\delta_{Psummer}$) and minimum ($\delta_{Pwinter}$) of the sine wave curve fitted to the $\delta^{18}O_{precipitation}$ values. For this purpose, a non-linear least square fitting algorithm was used in *R* utilizing the nls() function from the *stats* package, using a moving window algorithm on the $\delta^{18}O_{precipitation}$ to estimate the isotope amplitude over time. For clarity, $\delta^{18}O$ derived from the moving window sine wave fitting algorithm are referred to as δ_P, δ_Q, $\delta_{Psummer}$ and $\delta_{Pwinter}$, while original isotope data are referred to as $\delta^{18}O_{precipitation}$ and $\delta^{18}O_{streamwater}$.

To account for the interannual variability in the seasonal precipitation input signal from 1881 to 2023, we opted for a window size of 60 months, with time steps of 12 months. These windows run from June to June, aligning with the start of shell growth. With mean annual transit times in the Krycklan found to vary from 0.8 to 2.7 years and going up to 7.7 years in winter (Jutebring Sterte et al., 2021), these 5-year windows were meant to reflect the integrative nature of groundwater feeding the streams.

In the Krycklan reference catchment KRY C16, only 7 years of isotope measurements were available, making it unsuitable for the aforementioned protocol. Instead, a moving window algorithm with increasing window size and monthly time steps was selected for this case. The starting window size was first set to 24 months for the first years of the $\delta^{18}O_{precipitation}$ time-series and then increased by 12 months each time the number of observations permitted it. With this method, each $\delta^{18}O_{streamwater}$ value could be connected to the range and amplitude of the available precedent years of $\delta^{18}O_{precipitation}$ records.

2.5. Precipitation Oxygen Isotope Data ($\delta^{18}O_{precipitation}$)

Two complementary approaches were used to model $\delta^{18}O$ in precipitation at the bivalve sampling sites. The Piso.AI model by Nelson et al. (2021) uses a machine learning framework to predict monthly $\delta^{18}O$ in precipitation. It ranks the influence of several meteorological parameters on $\delta^{18}O_{precipitation}$ and has been calibrated against observations from the GNIP network, achieving an accuracy of RMSE of 1.7 ‰. The model is available online as a gridded data set (0.5°) covering Europe with monthly resolution from 1951 onward (available at https://isotope.bot.unibas.ch/PisoAI/; last access: 13 February 2025). The empirical model by Türk et al. (2025) was used to estimate $\delta^{18}O_{precipitation}$ based on location, temperature and atmospheric circulation patterns. Although its performance is slightly lower than that of Piso.AI (RMSE = 2.3 ‰), its minimal input requirements allowed $\delta^{18}O$ reconstructions back to 1881. Air temperature data was obtained from the Jokkmokk meteorological station (ECA station code: 1429; 66.63°N, 19.64°E, 254 m a.s.l.), accessed via the KNMI Climate Explorer (available at https://climexp.knmi.nl; last access: 13 February 2025). For the oldest shell-based $\delta^{18}O_{streamwater}$ proxy records, which

extend beyond 1881, we assumed invariant $\delta^{18}O_{precipitation}$ seasonality, using mean δ_P, $\delta_{Psummer}$ and $\delta_{Pwinter}$ values from the 1950—2000 reference interval, based on combined empirical and Piso.AI model data to calculate the SOI.

2.6. Bivalve-Based Reconstruction of Streamwater Oxygen Isotopes (δ_Q)

2.6.1. Shell Preparation

To obtain δQ data from mussels, shells were prepared using established sclerochronological methods, consistent with those employed by Schöne et al. (2020). The preparation process included evisceration of the animals, covering the shells with a protective layer of epoxy resin and obtaining two mirroring cross-sections of 2 and 3 mm thickness. These thick-sections were ground and polished with a series of abrasive SiC and Al_2O_3 powders with decreasing grain size (SiC: F800 and F1200 grit; Al_2O_3: 1 µm). The 2 mm section was used for shell growth pattern analysis enabling precise temporal alignment of isotope data. The 3 mm slab was used for micromilling powder samples for isotope measurements.

2.6.2. Isotope Analysis

Aragonite powder samples were obtained by milling the oOSL of the 3 mm shell section with a Rexim Minimo drill attached to a stereomicroscope. The sampling protocol is reported in detail in Schöne et al. (2020) and illustrated in the supplementary information of Gey et al. (2024). Oxygen isotope analysis of the carbonate powder was conducted using a Thermo Fisher Scientific MAT 253 isotope ratio mass spectrometer coupled to a GasBench II and operated in continuous flow mode. Samples of 50–120 µg were dissolved in anhydrous phosphoric acid at 72°C in He-flushed exetainers and the resulting CO_2 was analyzed for $\delta^{18}O$ values. A two-point calibration was performed using Carrara marble ($\delta^{18}O = 1.91‰$) and NBS-18 ($\delta^{18}O = -23.20‰$) as reference materials. IAEA 603 was used for quality control ($\delta^{18}O = -2.37‰$). Results are reported in δ-notation relative to the Vienna Pee Dee Belemnite (VPDB) with an analytical precision of 0.05‰. The $\delta^{18}O_{shell}$ values were not adjusted for differences in acid fractionation factors of aragonite (samples) and calcite (standards), because the empirical paleothermometry equation by Grossman and Ku (1986) used to derive $\delta^{18}O_{streamwater}$ from $\delta^{18}O_{shell}$ data (see next section) was also based on uncorrected isotope data.

2.6.3. Resolving the Thermodynamic Relationship Between Shell and Streamwater $\delta^{18}O$

To derive $\delta^{18}O_{streamwater}$ data from $\delta^{18}O_{shell}$ values, we used the empirical equation by Grossman and Ku (1986), as described in Schöne et al. (2020) incorporating the VPDB–VSMOW scale correction by Gonfiantini et al. (1995).

$$\delta^{18}O_{streamwater} = \frac{19.43 - 4.34 \times \delta^{18}O_{shell} - T_{streamwater}}{-4.34} \quad (6)$$

Water temperature ($T_{streamwater}$) was linearly interpolated from air temperature, following the method presented in Schöne et al. (2020). Near-surface air temperature time-series for the period 1950—2023 were obtained from the ERA5 reanalysis data set, provided by the European Centre for Medium-Range Weather Forecasts (ECMWF) as part of the Copernicus Climate Change Service (C3S). For data prior to 1950, we used the NOAA-CIRES-DOE Twentieth Century Reanalysis Version 3 (20CRv3). Both data sets were accessed through the Royal Netherlands Meteorological Institute (KNMI) Climate Explorer (available at https://climexp.knmi.nl/; last access: 15 May 2024). An accurate age model to determine the precise timestamp for each isotope sample is thus necessary for selecting the correct temperature (i.e., during periods of shell growth exclusively) and solving Equation 6 (see description below).

2.6.4. Shell Growth Model and Temporal Alignment of Isotope Data

In northern Sweden, annual growth models of freshwater pearl mussels can be constructed with high accuracy due to clearly visible winter lines resulting from pronounced seasonal shifts between warm summers (periods of fast shell growth) and cold winters (minimal to no shell growth). To enhance the visibility of these annual growth lines, the 2 mm shell slabs were immersed in Mutvei's solution at 38°C for 20 min (Schöne et al., 2005). The stained slabs were photographed under an Olympus SZX16 stereomicroscope with sectoral (one quarter)

darkfield illumination, using a Canon EOS RP camera. The widths of the annual increments were measured from one winter line to the next, parallel to the longest axis of the prisms, as described by Dunca et al. (2005). To enhance the accuracy of the isotope time-series for the VDL1 catchment, we performed cross-dating on all 15 VDL1 shell specimens, using the R-based tool RingdateR (Reynolds et al., 2021). This resulted in a robust annual age model with an Expressed Population Signal (EPS) of 0.87. However, errors can occur in shells of old-grown bivalves because annual increment widths decrease exponentially with ontogenetic age. In the studied streams of northern Sweden, these widths can exceed 800 µm during the first years of life, but narrow to less than 10 µm in old individuals, which can lead to time-averaging and temporal misalignment. To address this issue, $\delta^{18}O_{shell}$ values of VDL1-A7 after 1960 and of GJ-A3L were excluded from further analysis.

Although this study uses one $\delta^{18}O_{streamwater}$ value per annual growth increment representing the growing season, this value is derived from several sub-seasonal measurements. Therefore, a higher-resolution growth model is necessary to resolve individual shell isotope samples at shorter intervals, because sub-seasonal water temperature variations are key to accurately solve Equation 6. The VDL1 oxygen isotope data were temporally aligned using the monthly growth model of Gey et al. (2023, 2024). Previously published $\delta^{18}O_{streamwater}$ time-series by Schöne et al. (2020) from NJB, GTB and GJ have not been modified. They were aligned using a different growth curve established by Dunca et al. (2005). According to both models, more than 70% of the annual increment forms between June and August. The main difference is that the model by Dunca et al. (2005) assumes that the timing and rate of seasonal growth remained nearly unchanged throughout the lifetime of a specimen, while the model by Gey et al. (2023, 2024) dynamically predicts the growing season dependent on the water temperature in the respective year. For an average year at the VDL1 site, 23% of the annual increment forms in June, 52% in July and 25% in August. In warmer years, when the monthly average temperature exceeds 9°C, growth can already begin in May and extend into September. As a result, Dunca et al. (2005) predicted a longer growing season that starts at temperatures above 5°C, while Gey et al. (2023, 2024) suggested that growth was limited to temperatures above 9°C.

3. Results

3.1. SOI and Its Relationship to Streamflow and BFI at the Reference Catchment (Proof-of-Concept)

At the reference site of the Krycklan catchment, the annual median $\delta^{18}O_{precipitation}$ ranged from −13.7‰ to −13.2‰ during the observation period (January 2016–September 2023). We found a distinct seasonal pattern in $\delta^{18}O_{precipitation}$, with higher values in summer (JJA: −10.0‰ to −9.4‰) and lower values in winter (DJF: −17.6‰ to −16.8‰, Figure 2c). The annual median $\delta^{18}O_{streamwater}$ varied less, ranging from −13.5‰ (in 2022) to −13.0‰ (in 2016). The amplitude in $\delta^{18}O_{streamwater}$ was damped relative to $\delta^{18}O_{precipitation}$, with an interquartile range (IQR) of 0.6‰ for streamwater and 6.8‰ for precipitation. Occasional shifts toward more negative values (minimum −15.0‰) were observed in the streamwater during the spring snowmelt.

The streamflow behavior was clearly seasonal and dominated by snowmelt. The lowest specific discharge values occurred in winter (DJF: mean 29.5 mm), which were followed by high values in spring (MAM: mean 126.0 mm) with large peak flow events, characteristic of the subarctic regions (Figures 2a and 2b). Mean specific discharge values were also slightly higher in fall (SON: 55.1 mm) than in summer (JJA: 47.8 mm). In the reference KRY C16 catchment, the seasonal differences of the specific discharge based on direct hydrometric measurements were however less pronounced. Note that the discontinuities in the discharge measurements in KRY C16 due to snow cover in the winter reduced the sample size, especially in DJF. Specific discharge values laid around the median of 0.95 mm day^{-1} and baseflow values around the median of 0.34 mm day^{-1}, resulting in a median of daily BFI of 41%.

The SOI ranged from −0.38 to +0.39, with a median value of 0.06. Beginning in late spring (April–May) the SOI remained predominantly negative (median: −0.06) before becoming systematically positive in summer (0.15) and fall (0.16; Figure 3). This shift of the SOI values coincided with the strong seasonal variation in discharge. SOI values were significantly correlated to daily discharge and corresponding BFI (Figure 4). However large inter-annual and intraseasonal differences were observed, particularly in April, May and July (Figure 3). Moderate correlations of the SOI with the BFI values were found for all seasons, positive in spring (Pearson's $r = 0.58$, $p < 0.01$) and negative in summer ($r = -0.53$, $p < 0.01$) and fall ($r = -0.48$, $p < 0.01$). The relationship of specific discharge and SOI values was even stronger in spring ($r = -0.68$, $p < 0.01$), but weaker in summer ($r = 0.32$, $p = 0.06$) and non-significant in fall.

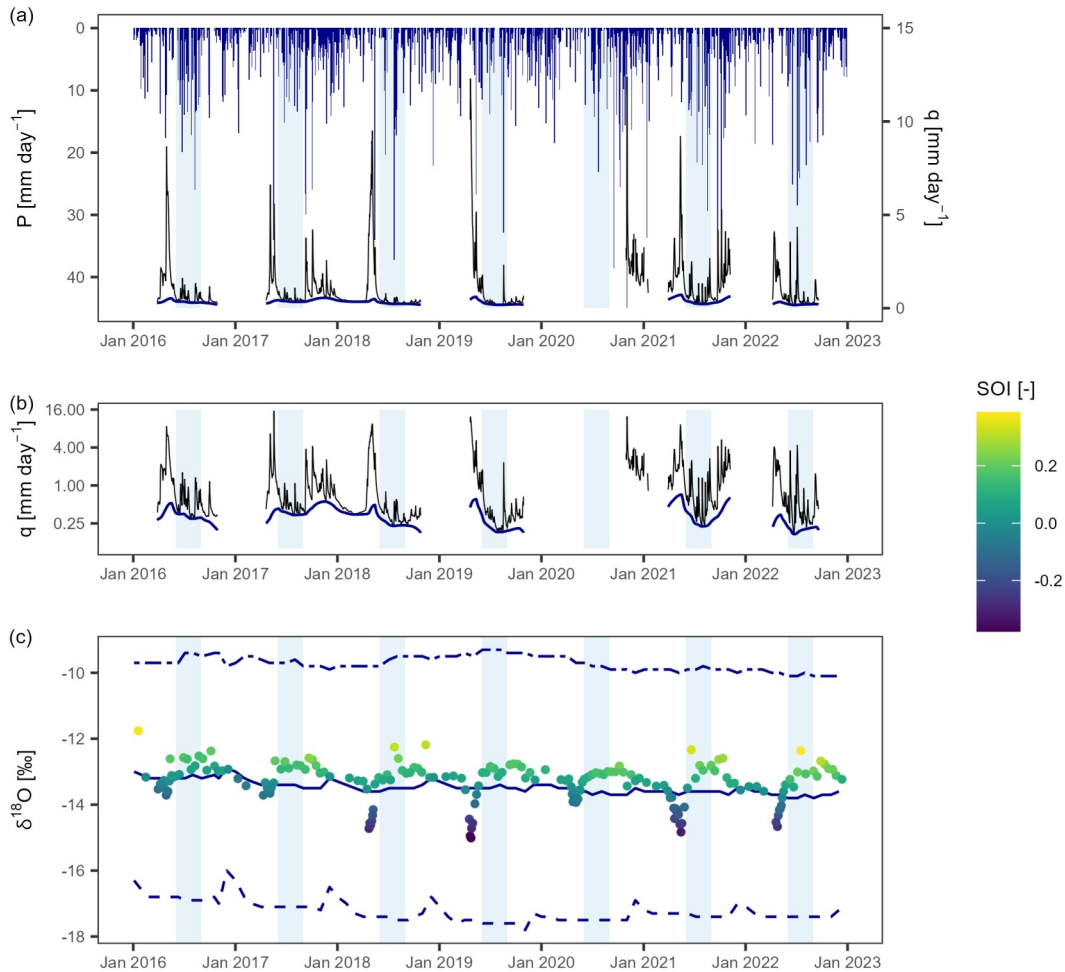

Figure 2. (a) Daily observations of precipitation (dark blue columns) and streamflow (black lines) at the KRY C16 reference site. Baseflow lines (dark blue lines) are also shown. Discontinuities indicate periods with lack of records due to ice cover. The main growth season (JJA) is indicated in light blue shading. (b) Streamflow and baseflow on a log-scale. (c) Sub-monthly $\delta^{18}O$ observations in streamflow (colored circles) and derived metrics in precipitation (δ_P, solid line; $\delta_{Psummer}$, upper dashed line; $\delta_{Pwinter}$, lower dashed line), obtained with a sine wave fitting algorithm. The SOI was calculated for $\delta^{18}O_{streamflow}$ observations and the signs colored accordingly.

3.2. Model-Derived Precipitation Oxygen Isotope Data (δ_P, $\delta_{Psummer}$, $\delta_{Pwinter}$)

Both $\delta^{18}O_{precipitation}$ models agreed well with the monitoring data at the reference site KRY C16 during the overlapping time interval (January 2014–December 2020), with strong correlations for the monthly averages with the empirical model of Türk et al. (2025) (Pearson's $r = 0.82$, $p < 0.001$) and Piso.AI (Nelson et al., 2021) ($r = 0.88$, $p < 0.001$). For the bivalve sampling sites, $\delta^{18}O_{precipitation}$ estimates (based on the empirical model) were similar for all four catchments (Figure 5a, Figure S1 in Supporting Information S1). Median δ_P values ranged from −13.1‰ (GJ/NJB) and −12.8‰ (VDL1), which lies within the model error of ±0.3‰. Notably, for δ_P (analog for $\delta_{Psummer}$; $\delta_{Pwinter}$) the error of ±2.3‰ for monthly $\delta^{18}O_{precipitation}$ values is reduced to ±0.3‰ when applying a sine wave curve fitting over a 5-year moving window (60 monthly observations). Median $\delta_{Psummer}$ varied between −9.5 ‰ (GJ/NJB) and −9.2‰ (VDL1) and $\delta_{Pwinter}$ between −16.6‰ (NJB) and −16.3‰ (VDL1). In all four locations, IQR of δ_P and $\delta_{Psummer}$ were narrow and ranged between 0.2 and 0.4‰ and IQR of $\delta_{Pwinter}$ were slightly broader and fluctuated between 0.7 and 0.8‰.

In contrast, Piso.AI-based δ_P values differed between the four catchments (Figure 5a, Figure S1 in Supporting Information S1). Still, median δ_P was close to the empirical model outputs, with values between −13.2‰ (GJ, GTB) and −13.0‰ (VDL1). This range lies within the adapted model error of ±0.2‰, which is reduced from the original ±1.7‰ for individual monthly $\delta^{18}O_{precipitation}$ values using the same 5-year moving window

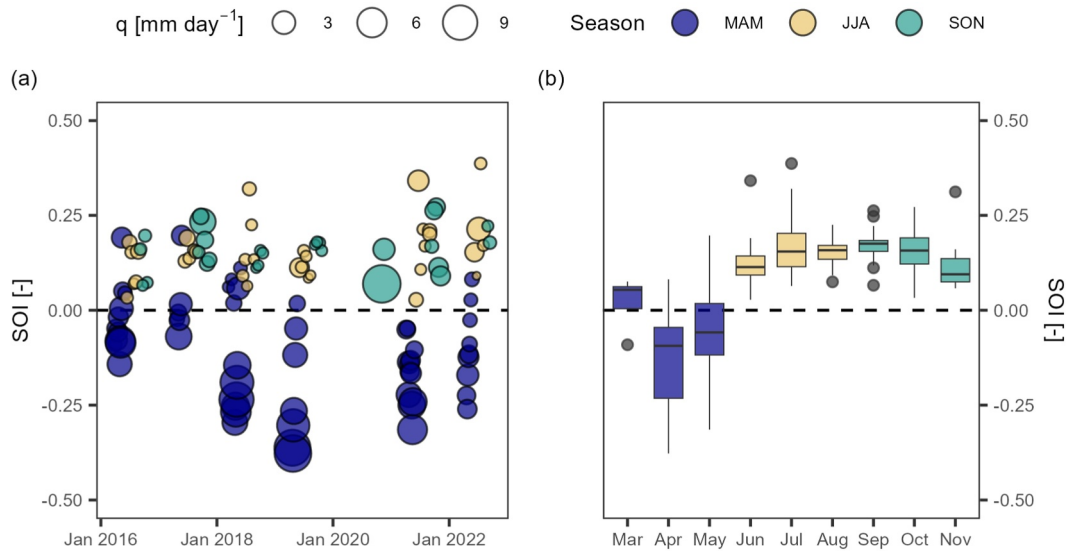

Figure 3. Left: Seasonal Origin Index (SOI) from January 2016 to September 2022 based on $\delta^{18}O_{streamwater}$ and $\delta^{18}O_{precipitation}$ data from the KRY C16 reference site, with bubble size representing specific discharge rates (daily, on the day of the grab samples in the stream) and color indicating the season. Summer (JJA) is the main shell-growing season of the freshwater mussel shells. Due to a lack of observations, the winter period was excluded. Right: Boxplots of SOI values regrouped by month, illustrating the seasonal variation of the SOI over the observation period.

procedure applied in the empirical model. Looking at the interannual variation of the seasonal signal, $\delta_{Psummer}$ and $\delta_{Pwinter}$ values exhibited a larger variation than the empirical model, that is, −10.7‰ (NJB) to −10.1‰ (GJ, GTB) in summer and −16.2‰ (GJ, GTB) to −15.4‰ (NJB) in winter. According to Piso.AI, the seasonal amplitude of $\delta^{18}O_{precipitation}$ was smaller at NJB and VDL1 than at GJ and GTB (Figure S1 in Supporting Information S1). The IQR of δ_P and $\delta_{Psummer}$ varied between 0.2 and 0.6‰ and IQR of $\delta_{Pwinter}$ between 0.9 and 1.3‰.

During the overlapping period from 1950 to 2018, the RMSE of δ_P estimated with the two models ranged between 0.4‰ (NJB, VDL1) and 0.5‰ (GJ, GTB). Model estimate differences of seasonal signals were more pronounced, with higher estimated empirical model $\delta_{Psummer}$ (RMSE between 0.8‰, GJ and 1.3‰, NJB) and lower $\delta_{Pwinter}$ (RMSE between 1.0‰ [GJ, GTB] and 1.4‰ [NJB, VDL1]). In general, differences were more pronounced for NJB and VDL1 than for GJ and GTB. The main reason for these differences lies in the empirical model showing

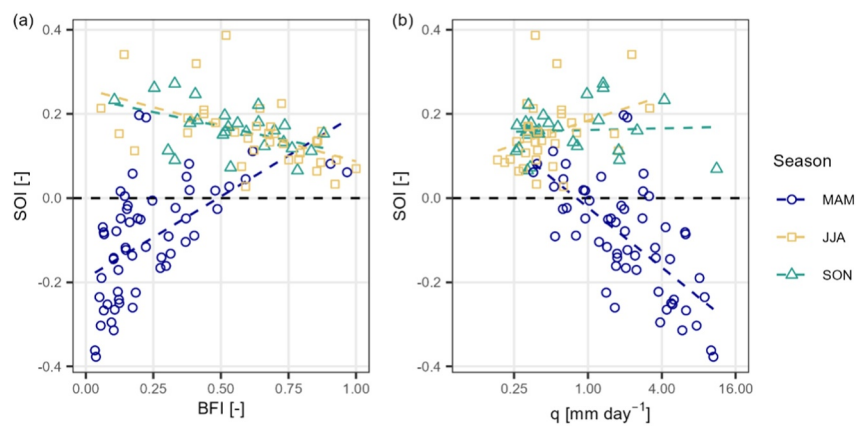

Figure 4. Scatterplots of the relationship between the SOI and the BFI (a) and the specific discharge (b) in the KRY-C16 reference site. Symbol color and shape indicate the season: spring (MAM), summer (JJA) and fall (SON). Regression lines show opposing trends in the MAM and in the JJA season.

10.1029/2025WR041632

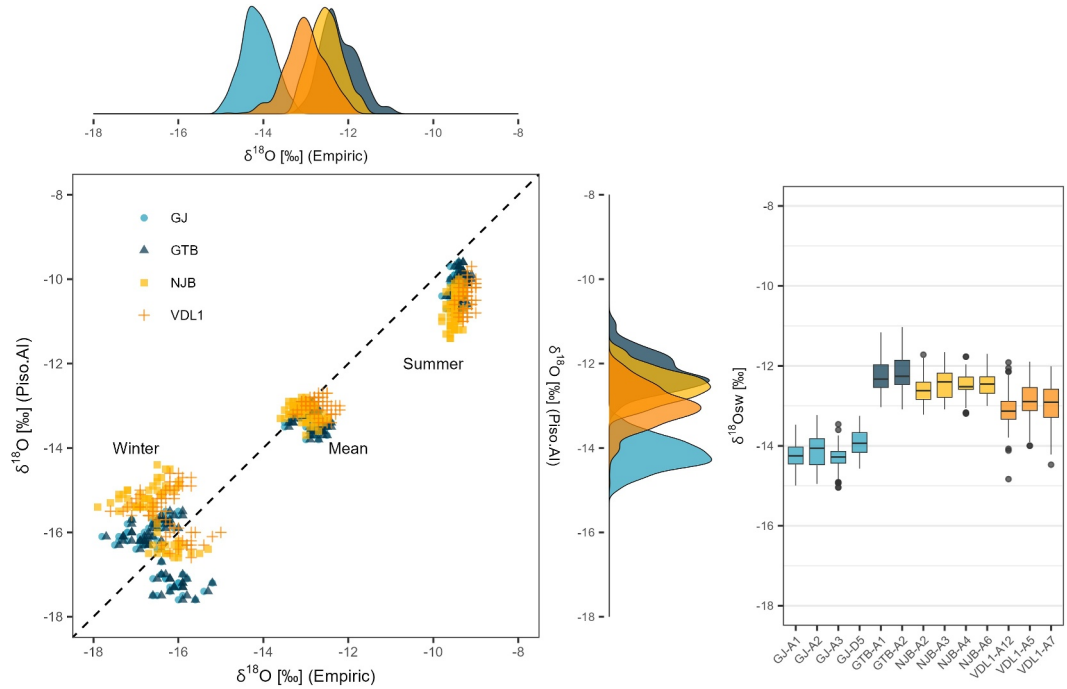

Figure 5. Left: Precipitation isotope signals (δ_P, $\delta_{Psummer}$, $\delta_{Pwinter}$) obtained with monthly $\delta^{18}O_{precipitation}$ from the empirical model plotted against estimations with Piso.AI, colored after the locality. The precipitation isotope signals were obtained with the 5-year moving sine wave fitting algorithm. The density plots on both sides of the plot represent the distribution of shell-derived $\delta^{18}O_{streamwater}$ in all four localities (represented by colors). Right: boxplots of shell-derived $\delta^{18}O_{streamwater}$ for individual bivalve specimens collected at the four sites.

more consistent variation of isotope amplitudes at all sites, while Piso.AI estimates had smaller amplitudes, with a sudden shift in the 2000s, particularly for $\delta_{Pwinter}$ (Figure S1 in Supporting Information S1). Only weak to moderate correlations were found between estimates from the two precipitation isotope models. These differences were negative for δ_P and $\delta_{Pwinter}$ (Pearson's $r = -0.45$–-0.37, $p < 0.002$, not significant for VDL1) and positive for $\delta_{Psummer}$ ($r = 0.25$–0.35, $p < 0.041$). Model estimate divergences thus seem to be more pronounced in summer. Relatively small differences of the model estimates (RMSE of less than 1.4‰, but low correlation strengths) also indicate that the models might not react to the same drivers. This led to phases where the model estimates are offset (see Figure S1 in Supporting Information S1).

3.3. Shell-Based Streamwater Oxygen Isotope Data (δ_Q)

Prior to the conversion of shell $\delta^{18}O$ values to $\delta^{18}O_{streamwater}$, the raw $\delta^{18}O_{shell}$ measurements ranged from −15.5 to −7.7‰. Significant differences were found between the catchments for the overlapping time interval of 1943–1993 (Kruskal-Wallis test, $p < 0.001$), with median $\delta^{18}O_{shell}$ values for VDL1 of −10.6‰ (IQR = 0.7‰), NJB of −9.8‰ (IQR = 0.6‰) and GTB of −9.6‰ (IQR = 0.7‰). In contrast, GJ exhibited a distinctly lower $\delta^{18}O_{shell}$ median of −11.5‰ and a narrower IQR of 0.5‰. Median $\delta^{18}O_{shell}$ values among bivalve specimens from the same sampling locality showed minimal variation, with maximum differences below 0.2‰.

Comparing annually resolved $\delta^{18}O_{shell}$ time-series, varying correlation strengths were detected between isotope signals from specimens from the same sampling site. At VDL1, a moderate correlation was observed between shells A5 and A12 ($r = 0.72$, $p < 0.001$), but no significant correlations with the other specimens for specimen A7. This aligns with findings by Schöne et al. (2020) for the sites GTB, NJB and GJ, reporting generally moderate to strong correlations between shells from the same stream, with weak or no significant correlations for only some specimens.

Reconstructed $\delta^{18}O_{streamwater}$ values ranged from −11.0 to −15.0‰. Inter-catchment differences in $\delta^{18}O_{streamwater}$ mirrored those observed for $\delta^{18}O_{shell}$. Median $\delta^{18}O_{streamwater}$ in VDL1 (−12.5‰, IQR = 0.7‰), NJB (−12.5‰,

Table 2
Median Seasonal Origin Index (SOI) With the Interquartile Range (IQR) Derived From Modeled δP and Shell-Derived δQ for Each Sampling Site

	SOI (IQR)			
			Model comparison	
Stream ID	Full record	Overlap (1946–1993)	Empirical	Piso.Ai
VDL1	−0.05 (0.24)	−0.05 (0.24)	−0.06 (0.19)	+0.00 (0.26)
NJB	+0.19 (0.20)	+0.19 (0.20)	+0.17 (0.14)	+0.21 (0.31)
GTB	+0.26 (0.22)	+0.27 (0.21)	+0.20 (0.16)	+0.32 (0.22)
GJ	−0.31 (0.24)	−0.33 (0.25)	−0.31 (0.24)	−0.36 (0.24)

Note. SOI over the full record is prior to 1951 based on δ_P values from the empirical model of Türk et al. (2025) and after 1951 based on the average δ_P from both the empirical model and Piso.AI. The period of overlap, where SOI data are available for all shell sampling sites, covers the years 1946–1993. Model comparison is based on the full timespan covered by the shells after 1951, where both δ_P models are available.

IQR = 0.5‰) and GTB (−12.3‰, IQR = 0.6‰) differed little, while GJ exhibited notably lower values (−14.1‰, IQR = 0.5‰) (Figure 5, Figure S1 in Supporting Information S1). The $\delta^{18}O_{streamwater}$ chronologies from GTB, GJ and NJB were moderately correlated ($r = 0.59$–0.61, $p < 0.05$), while VDL1 showed no significant correlations with the other sites. The use of different seasonal growth models for $\delta^{18}O_{streamwater}$ reconstructions in VDL1 showed that the Dunca et al. (2005) model predicts average annual $\delta^{18}O_{streamwater}$ 0.6‰ higher than the Gey et al. (2023, 2024) model.

3.4. Reconstructed SOI Chronologies

We found marked differences in the SOI among the four streams (Kruskal-Wallis test; $p < 0.001$) (Table 2; Figure 6), with median values ranging from −0.36 (GJ, Piso.AI) to +0.32 (GTB, Piso.AI) between 1890 and 2020. The SOI in GJ and VDL1 was persistently negative (except for SOI based on A7 shell in VDL1) and persistently positive in NJB and GTB. Median SOI (averaging SOI obtained with the empirical model and Piso.AI after 1950) were high in both GTB (+0.27, IQR = 0.18) and NJB (+0.2, IQR = 0.25). In VDL1, SOI were close to the null line, with a median of −0.05 (IQR = 0.18) and SOI were clearly negative in GJ, with a median of −0.30 (IQR = 0.18).

The RMSE between the SOI obtained using the empirical model and Piso.AI for $\delta^{18}O_{precipitation}$ estimations at the four locations ranged between 0.09 (GJ) and 0.14 (NJB, VDL1). Although the overall SOI based on the empirical model was 0.04 higher than that from Piso.AI, its range was narrower (IQR = 0.39, empirical model; IQR = 0.51, Piso.AI). Correlations between the SOI obtained with the two models were high for all catchments ($r = 0.76$–0.93, $p < 0.001$). Unlike the $\delta^{18}O_{streamwater}$, strongly correlated with the SOI ($r = 0.95$, $p < 0.001$), variables derived from $\delta^{18}O_{precipitation}$ (δ_P, $\delta_{Psummer}$, $\delta_{Pwinter}$) showed very weak or no significant correlations with the SOI. On the temporal scale, mean δ_P, $\delta_{Psummer}$ and $\delta_{Pwinter}$ for the reference period (1950–2000) instead of varying values for the SOI calculations resulted in a RMSE of 0.06, with a strong correlation between the signals ($r = 0.97$, $p < 0.001$). This allowed an extension of the reconstructions beyond 1882, when the empirical model-based $\delta^{18}O_{precipitation}$ end, up to 1836, where the oldest shell-derived $\delta^{18}O_{streamwater}$ originated from (shell VDL1-A7, Figure 6).

Analysis of the SOI time-series revealed a decreasing trend in GJ from ca. 1880 to 1980, followed by a pronounced shift to higher values until the end of the record in 1999. Similarly, the SOI at NJB followed a positive trend after 1980. In contrast, GTB and VDL1 showed no significant long-term tendencies (Figure 6). Shell-based SOI in GJ exhibited significant correlations ranging from moderate to strong ($r = 0.48$–0.82, $p < 0.003$), with shell A3 having the weakest correlations among them. In GTB, shells A1 and A2 exhibited a moderate correlation ($r = 0.45$, $p = 0.002$). NJB demonstrated the highest consistency, with all four shells being strongly correlated ($r = 0.75$–0.98, $p < 0.001$), with shell A4 having the weakest relationship with other shell SOI. In VDL1, only SOI from the shells A5 and A12 were significantly correlated ($r = 0.76$, $p < 0.001$), A7 deviated significantly from the two others.

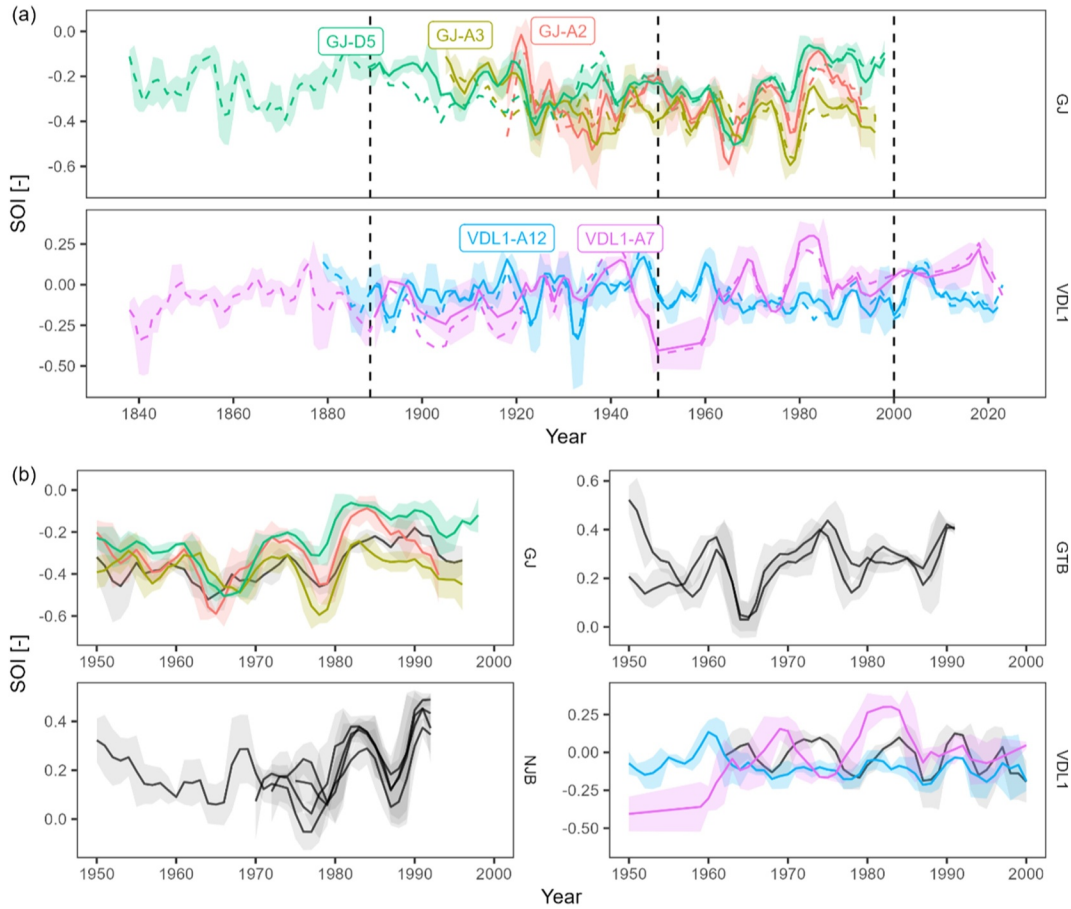

Figure 6. Time-series of the shell-based SOI (a) from 1836 to 2022 for long-lived shells in GJ and VDL1 and (b) in all catchments from 1950 to 2000. The lines represent running means calculated using 3-year windows with standard deviations given as shadings. Before 1950, the solid lines are based on the empirical model only. After 1950, they are the average of the empirical model and Piso.AI outputs. The dashed lines are SOI reconstructions assuming constant $\delta^{18}O_{precipitation}$ from the reference period 1950–2000.

4. Discussion

4.1. Reliability of Centennial Shell-Based SOI Reconstructions

In this paper, we show that centennial chronologies of seasonal origins in streamwater (SOI) can be reconstructed utilizing shell-based streamwater $\delta^{18}O$ time-series. The oldest SOI records reconstructed here go back to the year 1836 for two locations, while other multi-decadal time-series were obtained for four locations in northern Sweden. Before moving to the interpretation of long-term SOI signals, it is important to understand the robustness and the sensitivity of these reconstructions. Through this rigorous uncertainty assessment, we conclude that centennial SOI chronologies can be reliably reconstructed from model-derived precipitation $\delta^{18}O$ data and sclerochronology-based streamwater $\delta^{18}O$, thus verifying our first hypothesis.

4.1.1. Robustness of Shell-Derived $\delta^{18}O_{streamwater}$

The robustness of reconstructing stream water oxygen isotopes from bivalve shells depends on three key factors: (a) oxygen near-equilibrium biomineralization in the selected species and shell portion with the ambient water, (b) accurately estimating the water temperature to apply the thermodynamic relationship between $\delta^{18}O_{shell}$ and $\delta^{18}O_{streamwater}$ and (c) developing a precise age model to contextualize each powder sample in time and ensure correct temperature attribution during shell formation.

Biomineralization near oxygen isotope equilibrium with ambient water has been confirmed for *Margaritifera margaritifera* in multiple studies (Gey et al., 2024; Schöne et al., 2020). In tank experiments under controlled, constant temperature conditions, the study by Gey et al. (2024) quantified a 0.5‰ deviation from the shell-derived median values and the in situ water oxygen isotope data. This uncertainty is significantly smaller than those of precipitation isotope models (e.g., PISO.ai RMSE = 1.7‰; Türk et al., 2025 RMSE = 2.3‰).

Field reconstructions also bring uncertainty from estimating water temperature at the time of shell formation to solve the thermodynamic relationship between $\delta^{18}O_{shell}$ and $\delta^{18}O_{streamwater}$. The transfer functions that leverage the strong correlation between air and water temperatures are oblivious of the great heterogeneity characterizing the streams. For instance, varying groundwater contributions can impact the temperature relationship (Anderson, 2005). Regional calibrated air to water temperature transfer functions may not provide equally accurate approximations for all streams, or even shells in different stream sections. This calls for a close inspection of the magnitude of temperature effects on reconstructed $\delta^{18}O_{streamwater}$. Using the thermodynamic relationship between $\delta^{18}O_{shell}$ and $\delta^{18}O_{water}$ given in Equation 6, temperature change of about 2°C would result in an isotope difference of about 0.5 ‰ in the shell-based $\delta^{18}O_{streamwater}$ reconstructions. IQR in all four locations were roughly within that range, which calls for a cautious interpretation of the temporal variation in $\delta^{18}O_{streamwater}$ signals and derived SOI chronologies. However, an isotope difference of 1.9 ‰ between the shell-based $\delta^{18}O_{streamwater}$ reconstructions, as seen for example, between GTB and GJ, would imply a contrast of 8°C between the streams to be a temperature-induced artifact. Given that the catchments are only 80 km from each other and have similar elevation spans (ca. 90–200 m a.s.l.), such a large temperature difference cannot plausibly explain this $\delta^{18}O_{streamwater}$ variation. Only the small difference in $\delta^{18}O_{streamwater}$ reconstructions between NJB and GTB falls within the uncertainty range caused by inaccuracies in water temperature estimates.

Lastly, uncertainty arises from the use of different seasonal growth models. Although the two used growth models predict a similar main growing season between June and August, the Dunca et al. (2005) model systematically results in annual $\delta^{18}O_{streamwater}$ values that are approximately 0.6‰ higher compared to those derived with the Gey et al. (2023, 2024) model. The temperature-based model by Gey et al. dynamically adapts to annual temperature variations, providing greater precision. However, while tank experiments confirm a very strong correlation between growth and temperature ($r = 0.99$; $p = 0.011$; Gey et al., 2023), natural growth conditions are also affected by factors such as food availability (Mutvei et al., 1996; Schöne et al., 2004) and pH (Ninokawa & Ries, 2022). Accordingly, the daily increment-counting approach by Dunca et al. may offer a more realistic estimate of subannual growth by reflecting the combined influence of all growth determinants. However, its static nature, relying on specific years to extrapolate for all years, limits its adaptability. Additionally, the model assumes similar regional growth conditions, even though pH and food availability can vary significantly between streams, potentially diminishing its advantage over the temperature-based model. As a result, the accuracy of each model may vary depending on the environmental conditions of a given year, making them individually better suited for different contexts.

4.1.2. Sensitivity of SOI Reconstructions

The reconstructed SOI chronologies (Figure 6) revealed distinct patterns including (a) deviations over certain periods depending on the $\delta^{18}O_{precipitation}$ model, (b) co-variance of SOI signals derived from different shells at the same locality attributed to overarching hydrological signals and (c) punctual divergences of SOI chronologies from individual shells from the predominant signal, either biogenically driven or by different microenvironmental conditions experienced by the mussels. To disentangle hydrologic signals from other patterns, resolving these uncertainties is critical.

Calculation of the SOI (Equation 5) is sensitive to $\delta^{18}O_{precipitation}$ inputs, as small variations in the denominator ($\delta_{Psummer}$–δ_P or δ_P–$\delta_{Pwinter}$, depending on δ_Q) can introduce significant fluctuations in SOI values, particularly when $\delta_{Psummer}$ or $\delta_{Pwinter}$ approaches δ_P. The large seasonal contrast of $\delta^{18}O_{precipitation}$ in the studied region is therefore of advantage for the robustness of the SOI. However, differences in model derived metrics, particularly the seasonal isotope signals ($\delta_{Psummer}$, $\delta_{Pwinter}$), lead to noticeable variations in the SOI. While the empirical model shows a more consistent variation of isotope amplitudes at all sites, Piso.AI exhibits a narrower amplitude, with a sudden shift in the 2000s (Figure S1 in Supporting Information S1). Consequently, uncertainties in δ_Q (as discussed in Section 4.1) have a tendentially larger effect on the SOI based on the Piso.AI model, especially before the year 2000, because the amplitude is smaller.

Determining which model performs more reliably under these circumstances remains challenging. Piso.AI, which incorporates a broader set of input variables, may better capture regional isotope effects. For example, the inclusion of convection strength sensibly improves the ability to capture isotope variability (Türk et al., 2025). This could have led to the low correlation strengths between the precipitation isotope model estimates, particularly in summer. Still, the accuracy of $\delta^{18}O_{precipitation}$ models in Scandinavia, especially Sweden, may be limited due to sparse $\delta^{18}O_{precipitation}$ data, with GNIP records from northern Sweden being only available for the period 1975–1980. Despite these differences, both models produce broadly consistent SOI signals (RMSE = 0.09–0.14). Our results also showed that averaging isotope signals from both models across the overlapping interval from 1950 to 2000 instead of taking varying values resulted in relatively small alterations of the SOI (RMSE = 0.06). Hence, the influence of weakly correlated $\delta^{18}O_{precipitation}$ model estimates on resulting SOI variability might be negligeable, although it may obscure inter-annual hydrological variability.

Beyond $\delta^{18}O_{precipitation}$ model-related uncertainties, biogenically driven inter-shell differences in reconstructed $\delta^{18}O_{streamwater}$ (δ_Q) within the same stream add complexity to SOI chronologies (Figure 6). Such variations arise when actual shell growth deviates from the expected seasonal growth curve, introducing temporal alignment uncertainties within the error margins of the growth model (as discussed in Section 4.1). These misalignments affect temperature assignments when converting $\delta^{18}O_{shell}$ to $\delta^{18}O_{streamwater}$ (Equation 6). This uncertainty increases with the ontogenetic growth trend: as bivalves age, annual increments become narrower, reducing sampling density and the precision of seasonal alignment. Consequently, sampling sites with younger specimens, such as NJB and GTB (with shells aged 25 and 52 years, respectively), exhibit higher consistency across SOI series. In contrast, older bivalves from GJ provide fewer samples per increment toward the end of their lifetimes, resulting in slight heteroscedasticity across the SOI chronologies starting around 1960. Despite these uncertainties, the GJ SOI chronologies exhibit strong overall congruence on a decadal scale, allowing for hydrological interpretations (detailed in Section 4.3).The use of multiple SOI chronologies is crucial for a more robust interpretation, as individual specimens can show punctual deviations from the predominant SOI signal (e.g., GJ-D5 (1930–1940), NJB-A4 (1975–1978), VDL1-A7 (1967–1977)). These deviations can be attributed to microhabitat differences within the streams. For example, at the VDL1 sampling site, habitat conditions varied along approximately 50 m: An upstream section dominated by sand and gravel, where mussels were evenly distributed across the streambed and a downstream section characterized by rocks and boulders, where mussels occupied small sand and gravel patches between rocks. Such differences in the riverbed can affect water turbulence, oxygen concentration and food availability, which can individualize the growth curves of the shells depending on the microhabitat (Dunca et al., 2005; Hastie et al., 2000; Mutvei et al., 1996). One should also be aware that microhabitat conditions tend to change over the multi-decadal lifetime of the bivalves and that the shell growth may be affected by local disturbances of their immediate environment. While *Margaritifera margaritifera* has been observed moving up to 3 m in 24 hr during simulated drawdown events to avoid exposure to air (Curley et al., 2022), such extreme behavior is unlikely in northern Sweden, where mussels generally inhabit deeper waters to avoid freezing in winter (Hastie et al., 2000). Still, even small movements to find favorable conditions (Eissenhauer et al., 2023) or prioritization for reproduction (Bauer, 1998), or responses to injury, disease or parasite infestation (e.g., Alfjorden et al., 2024), could divert energy from biomineralization leading to further alterations of the $\delta^{18}O_{shell}$ record.

Lastly, the $\delta^{18}O_{streamwater}$ signature itself could also be heterogeneous on a small spatial scale. For example, individual mussels may access water from different sources within the same stream, such as groundwater inflows near the streambed with distinct isotope signatures compared to more mixed signatures from different sources in the central channel sections (Peralta-Tapia et al., 2015). While these patchy differences can cause short-term variations, they are generally transient due to stream mixing processes that homogenize isotope signatures over time. Consequently, long-term SOI patterns remain largely unaffected, especially when multi-year moving averages smooth out transient fluctuations.

4.2. SOI as a Metric to Understand Summer Low-Flow Conditions

Snow-rich winters, dynamic spring runoff and low-flow conditions during summer and fall shape the SOI for the streams of northern Sweden. At the reference catchment KRY C16, the spring flood peak results in negative SOI values from March to May due to rapid snowmelt, which releases little under 50% of annual precipitation into the stream. These snowmelt inputs with strongly negative SOI signatures at high streamflow contrast with baseflow

conditions, which is reflected in a moderate positive correlation between SOI and BFI (Pearson's $r = 0.58$, $p < 0.01$). In contrast, summer and fall are characterized by relatively low discharge and baseflow. Rainfalls with summer isotope signatures drive the SOI up, remaining generally positive. During this period, a significant negative correlation is observed between SOI and BFI ($r = -0.53$, $p < 0.01$). This is because the growing contribution of groundwater to baseflow, which is primarily recharged by snowmelt, that is, winter precipitation (Bishop et al., 2011; Laudon et al., 2007).

Bivalve-based SOI reconstructions also reflect these dynamics during the main shell growing season (June to August). GTB (median SOI +0.27) and NJB (median SOI +0.20) show a summer precipitation signature similar to KRY C16, indicating that streamflow in these catchments is responding relatively quickly to precipitation. In contrast, VDL1 shows a balanced seasonal contribution (SOI −0.05), while GJ stands out with a negative median SOI of −0.30, indicating a persistent winter precipitation signature even in summer. The notable increase in SOI from the mid-twentieth century also coincides with increasing annual precipitation, leading to a decline in drought frequency (Teutschbein et al., 2022), with less prolonged baseflow conditions in summer and more precipitation in summer feeding the stream. A similar increase in summer SOI has been identified in a Krycklan subcatchment upstream of KRY C16, based on a $\delta^{18}O_{streamwater}$ record spanning 2002–2022 (Tiwari & Laudon, 2025). The authors attributed this trend to enhanced mid-winter snowmelt, which increases winter discharge but reduces aquifer recharge. Consequently, groundwater contributions to summer streamflow decline relative to the increased influence of summer precipitation, which may represent an additional driver of rising summer SOI during recent decades. Along similar lines, GJ exhibits a declining SOI from around the beginning of the twentieth century to the end of the 1960s, which could reflect increasing winter contributions during that period. This pattern aligns with regional runoff declines in northern Sweden from 1920 to a minimum observed in the 1970s (Lindström & Bergström, 2004). Assuming GJ followed this regional trend, the declining SOI could be explained by streamflow deficits amplifying relative baseflow contributions, thereby strengthening the winter precipitation signal.

In contrast, VDL1 shows no distinct long-term trend but exhibits pronounced variability. Unlike GJ, which maintains a stable, baseflow-dominated regime from deeper groundwater sources, smaller catchments such as VDL1, NJB and GTB are more sensitive to drought. In these systems, baseflow likely depends on shallow groundwater, which is lowered during prolonged dry periods, leading to elevated SOI values as baseflow declines and evapotranspiration increases. These observations are a strong indication that reconstructed SOI chronologies capture long-term dynamics in summer low-flow conditions in boreal landscapes, also validating our second hypothesis. At the same time, the different dynamics in SOI timeseries in each catchment are an indication that physiographic characteristics are a cardinal control on long-term dynamics in summer low-flow conditions these regions.

4.3. Influence of Physiographic Characteristics on SOI Chronologies

While the four catchments share similar exposure to hydroclimatic changes, they exhibit unique hydrological responses, meaning that they are influenced by local physiographic characteristics—our third hypothesis. The systematically negative SOI values observed at GJ (Table 2; Figures 5 and 6) could be attributed to its substantially larger drainage area (215.8 km^2) compared to the other catchments (8.9–79.5 km^2; Table 1). Peralta-Tapia et al. (2015) found that larger subcatchments in the Krycklan exhibited greater ^{18}O depletion, indicating stronger contributions from deep groundwater. In contrast, smaller subcatchments carried the $\delta^{18}O$ signature of summer and fall precipitation. Tiwari et al. (2014, 2017) confirmed these findings, demonstrating that baseflow in larger catchments was primarily sourced from deeper groundwater.

However, catchment size may only partly explain the increased deep grondwater contribution. For example, Jutebring Sterte et al. (2021) instead emphasized the role of land cover soil characteristics. In the Krycklan, larger catchments tend to have greater silty sediment cover, which leads to longer reported water transit times. Smaller catchments are less silty and exhibit shorter transit times, suggesting that the relationship between catchment size and deep groundwater influence may not be purely causal. While all catchments in this study are dominated by till, GJ remains distinct, having the highest proportion of peatland cover (Figure 1). Peatlands retain older water in their dense, deep layers and integrate long-stored groundwater into streams (e.g., Jutebring Sterte et al., 2018, 2021; Karimi et al., 2024; Tetzlaff et al., 2015). In contrast, till-dominated systems such as GTB and NJB, with

less peat cover, presumably respond more directly to precipitation. In particular, numerical modeling, supported by oxygen isotope and cation tracer analyses (Jutebring Sterte et al., 2018, 2021), demonstrated that till with a higher horizontal hydraulic conductivity (2×10^{-5} m/s) promotes lateral subsurface flow and shorter transit times. Peat, however, has lower horizontal conductivity (1×10^{-5} m/s), but higher vertical conductivity (5×10^{-5} m/s), leading to slower lateral movement and prolonged water storage (Jutebring Sterte et al., 2018, 2021). Although macropores and less dense surface layers in peat can generate rapid shallow runoff under saturated conditions, this is unlikely to influence the bivalve-shell derived SOI in GJ, as shell growth likely occurs after the saturated conditions of the snowmelt season.

At VDL1, an additional factor likely influencing transit times, is the presence of two upstream lakes (3.5 and 2.0 km^2) located above the mussel sampling site. In the Krycklan catchment, Karlsen et al. (2019) observed that sub-catchments influenced by lakes and characterized by long, low-gradient flow paths exhibit higher dynamic storage. Such buffering can stabilize discharge and extend the contribution of winter precipitation to streamflow, which explains the SOI values close to zero at VDL1, indicating a balanced signal from both winter and summer precipitation.

5. Conclusion

This study presents the first multi-decadal reconstruction of the Seasonal Origin Index (SOI; Allen et al., 2019), derived from freshwater pearl mussel shell records of streamwater $\delta^{18}O$, combined with model-based precipitation $\delta^{18}O$ values over the two last centuries. The SOI quantifies the relative contribution of seasonal precipitation to streamflow, ranging from -1 (entirely winter-derived) to $+1$ (entirely summer-derived). Because freshwater pearl mussels grow annually from June to July, the shell-derived SOI reflects streamwater conditions during typical summer low-flow periods.

In the reference catchment, SOI during summer was negatively correlated with baseflow. This relationship arises because groundwater, which sustains baseflow, is in this region primarily recharged by winter precipitation, whereas summer rainfall generates the fast flow component. Thus, shell-derived SOI serves as an indirect indicator of baseflow contributions.

A thorough uncertainty assessment supports the robustness of the reconstructed SOI in capturing catchment-specific hydrological responses to precipitation variability, provided that seasonal precipitation isotope signatures are sufficiently distinct. We found that small headwater catchments (<40 km^2; NJB, GTB) had positive SOI values, indicating strong reliance on summer precipitation. A medium-sized catchment with upstream lakes (VDL1, 79.5 km^2) exhibited SOI values near zero, reflecting a balanced contribution of seasonal precipitation. The consistently negative SOI in the largest peat-rich catchment (GJ, 215.8 km^2) suggests that winter precipitation, stored and released as baseflow, sustains summer streamflow.

These insights from arbitrarily selected catchments open opportunities for further investigation, potentially serving as a foundation for systematic regional studies using long-lived mollusks to identify hydrological shifts at the catchment level. This study demonstrates that with the shells of freshwater bivalves, hydrological questions covering long-term effects influenced by climatic drivers can be addressed. The approach offers a scalable way to extend isotope baselines into pre-instrumental times, enabling model calibration and supporting adaptive water-resource management in data-scarce regions. The near-global distribution and ecological diversity of freshwater mollusks (for review see Lydeard & Cummings, 2019) make this approach globally relevant.

Conflict of Interest

The authors declare no conflicts of interest relevant to this study.

Data Availability Statement

Data and a metadata sheet are available in the Zenodo data repository under https://doi.org/10.5281/zenodo.15756303.

Acknowledgments
We thank Elin Bäckström and Malin Holmgren from the County Administrative Board of Västerbotten for field support and equipment provision. Special thanks to Michael Maus (JGU Mainz) for help with isotope measurements and Alessandro Aiello (JGU Mainz) and Tom Neder (JGU Mainz) for laboratory assistance as well as Katharina E. Schmitt for scientific feedback and support with QGIS. We thanks SITES and KAW 2023.0245 for providing Krycklan data. We also thank the reviewers and the Associate Editor for their constructive comments and careful evaluation of the manuscript. This study was made possible by a German Research Foundation (DFG) Grant (SCHO793/25) to B.R.S. and a Luxembourg Fonds National de la Recherche (FNR) Grant (C20/SR/14757154) to L.P. within the framework of the joint D-LUX—CORE 2020 project MUSES. Open Access funding enabled and organized by Projekt DEAL.

References

Ala-Aho, P., Autio, A., Bhattacharjee, J., Isokangas, E., Kujala, K., Marttila, H., et al. (2021). What conditions favor the influence of seasonally frozen ground on hydrological partitioning? A systematic review. *Environmental Research Letters*, *16*(4), 043008. https://doi.org/10.1088/1748-9326/abe82c

Alavi, G., Jansson, P.-E., Hällgren, J.-E., & Bergholm, J. (2001). Interception of a dense spruce forest, performance of a simplified canopy water balance model. *Hydrology Research*, *32*, 265–284. https://doi.org/10.2166/nh.2001.0016

Alfjorden, A., Onut-Brännström, I., Wengström, N., Kristmundsson, A., Jamy, M., Persson, B. D., & Burki, F. (2024). Identification of a new gregarine parasite associated with mass mortality events of freshwater pearl mussels *(Margaritifera margaritifera)* in Sweden. *The Journal of Eukaryotic Microbiology*, *71*(3), e13021. https://doi.org/10.1111/jeu.13021

Allen, S. T., von Freyberg, J., Weiler, M., Goldsmith, G. R., & Kirchner, J. W. (2019). The seasonal origins of streamwater in Switzerland. *Geophysical Research Letters*, *46*(17–18), 10425–10434. https://doi.org/10.1029/2019GL084552

Anderson, M. P. (2005). Heat as a ground water tracer. *Groundwater Series*, *43*(6), 951–968. https://doi.org/10.1111/j.1745-6584.2005.00052.x

Arheimer, B., Donnelly, C., & Lindström, G. (2017). Regulation of snow-fed rivers affects flow regimes more than climate change. *Nature Communications*, *8*(1), 62. https://doi.org/10.1038/s41467-017-00092-8

Arheimer, B., & Lindström, G. (2015). Climate impact on floods: Changes in high flows in Sweden in the past and the future (1911–2100). *Hydrology and Earth System Sciences*, *19*(2), 771–784. https://doi.org/10.5194/hess-19-771-2015

Bauer, G. (1998). Allocation policy of female freshwater pearl mussels. *Oecologia*, *117*(1–2), 90–94. https://doi.org/10.1007/s004420050635

Benettin, P., Rodriguez, N. B., Sprenger, M., Kim, M., Klaus, J., Harman, C. J., et al. (2022). Transit time estimation in catchments: Recent developments and future directions. *Water Resources Research*, *58*(11), e2022WR033096. https://doi.org/10.1029/2022WR033096

Bishop, K., Seibert, J., Nyberg, L., & Rodhe, A. (2011). Water storage in a till catchment. II: Implications of transmissivity feedback for flow paths and turnover times. *Hydrological Processes*, *25*, 3950–3959. https://doi.org/10.1002/hyp.8355

Curley, E. A. M., Thomas, R., Adams, C. E., & Stephen, A. (2022). Adaptive responses of freshwater pearl mussels, *Margaritifera margaritifera*, to managed drawdowns. *Aquatic Conservation: Marine and Freshwater Ecosystems*, *32*(3), 466–483. https://doi.org/10.1002/aqc.3759

Devito, K. J., Hokanson, K. J., Moore, P. A., Kettridge, N., Anderson, A. E., Chasmer, L., et al. (2017). Landscape controls on long-term runoff in subhumid heterogeneous Boreal plains catchments. *Hydrological Processes*, *31*(15), 2737–2751. https://doi.org/10.1002/hyp.11213

Dunca, E., Schöne, B. R., & Mutvei, H. (2005). Freshwater bivalves tell of past climates: But how clearly do shells from polluted rivers speak? *Palaeogeography, Palaeoclimatology, Palaeoecology*, *228*, 43–57. https://doi.org/10.1016/j.palaeo.2005.03.050

Eissenhauer, F., Grunicke, F., Wagner, A., Linke, D., Kneis, D., Weitere, M., & Berendonk, T. U. (2023). Active movement to coarse grained sediments by globally endangered freshwater pearl mussels (*Margaritifera margaritifera*). *Hydrobiologia*, *850*(4), 985–999. https://doi.org/10.1007/s10750-023-05138-1

Fan, Y., Clark, M., Lawrence, D. M., Swenson, S., Band, L. E., Brantley, S. L., et al. (2019). Hillslope hydrology in global change research and Earth system modeling. *Water Resources Research*, *55*(2), 1737–1772. https://doi.org/10.1029/2018WR023903

Gabrielli, C. P., & McDonnell, J. J. (2020). Modifying the Jackson index to quantify the relationship between geology, landscape structure, and water transit time in steep wet headwaters. *Hydrological Processes*, *34*(9), 2139–2150. https://doi.org/10.1002/hyp.13700

Gey, C. J., Pfister, L., Türk, G., Thielen, F., Leonard, L., Schmitt, K. E., & Schöne, B. R. (2024). Biologically driven isotope fractionation in ultrastructurally different shell portions of freshwater pearl mussels (*Margaritifera margaritifera*): Implications for streamwater δ18O reconstructions. *Limnology and Oceanography Letters*, *9*, 827–836. https://doi.org/10.1002/lol2.10426

Gey, C. J., Thielen, F., Pfister, L., Hissler, C., Türk, G., Baier, S., & Schöne, B. R. (2023). Disturbed by pH? Nacre tablet thickness of freshwater pearl mussels (*Margaritifera margaritifera*) is a poor temperature proxy. *Marine and Freshwater Research*, *74*(13), 1129–1144. https://doi.org/10.1071/MF23058

Gonfiantini, R., Stichler, W., & Rozanski, K. (1995). *Standards and intercomparison materials distributed by the International Atomic Energy Agency for stable isotope measurements (IAEA-TECDOC825)*. International Atomic Energy Agency (IAEA). Retrieved from https://www-pub.iaea.org/MTCD/publications/PDF/te_825_prn.pdf

Goodbrand, A., Westbrook, C. J., & van der Kamp, G. (2019). Hydrological functions of a peatland in a Boreal Plains catchment. *Hydrological Processes*, *33*(4), 562–574. https://doi.org/10.1002/hyp.13343

Grelle, A., Lundberg, A., Lindroth, A., Morén, A.-S., & Cienciala, E. (1997). Evaporation components of a boreal forest: Variations during the growing season. *Journal of Hydrology*, *197*(1–4), 70–87. https://doi.org/10.1016/S0022-1694(96)03267-2

Grossman, E. L., & Ku, T.-L. (1986). Oxygen and carbon isotope fractionation in biogenic aragonite: Temperature effects. *Chemical Geology*, *59*, 59–74. https://doi.org/10.1016/0168-9622(86)90057-6

Hastie, L. C., Young, M. R., & Boon, P. J. (2000). Growth characteristics of freshwater pearl mussels, *Margaritifera margaritifera* (L.). *Freshwater Biology*, *43*(2), 243–256. https://doi.org/10.1046/j.1365-2427.2000.00544.x

Intergovernmental Panel On Climate Change (IPCC). (2023). *Climate change 2022—Impacts, Adaptation and Vulnerability: Working Group II contribution to the sixth assessment report of the intergovernmental panel on climate change* (1st ed.). Cambridge University Press. https://doi.org/10.1017/9781009325844.3675.

Jutebring Sterte, E., Johansson, E., Sjöberg, Y., Huseby Karlsen, R., & Laudon, H. (2018). Groundwater-surface water interactions across scales in a boreal landscape investigated using a numerical modelling approach. *Journal of Hydrology*, *560*, 184–201. https://doi.org/10.1016/j.jhydrol.2018.03.011

Jutebring Sterte, E., Lidman, F., Lindborg, E., Sjöberg, Y., & Laudon, H. (2021). How catchment characteristics influence hydrological pathways and travel times in a boreal landscape. *Hydrology and Earth System Sciences*, *25*(4), 2133–2158. https://doi.org/10.5194/hess-25-2133-2021

Karimi, S., Maher Hasselquist, E., Salimi, S., Järveoja, J., & Laudon, H. (2024). Rewetting impact on the hydrological function of a drained peatland in the boreal landscape. *Journal of Hydrology*, *641*, 131729. https://doi.org/10.1016/j.jhydrol.2024.131729

Karlsen, R. H., Bishop, K., Grabs, T., Ottosson-Löfvenius, M., Laudon, H., & Seibert, J. (2019). The role of landscape properties, storage and evapotranspiration on variability in streamflow recessions in a boreal catchment. *Journal of Hydrology*, *570*, 315–328. https://doi.org/10.1016/j.jhydrol.2018.12.065

Karlsen, R. H., Grabs, T., Bishop, K., Buffam, I., Laudon, H., & Seibert, J. (2016). Landscape controls on spatiotemporal discharge variability in a boreal catchment. *Water Resources Research*, *52*(8), 6541–6556. https://doi.org/10.1002/2016WR019186

Katsuyama, M., Tani, M., & Nishimoto, S. (2010). Connection between streamwater mean residence time and bedrock groundwater recharge/discharge dynamics in weathered granite catchments. *Hydrological Processes*, *24*(16), 2287–2299. https://doi.org/10.1002/hyp.7741

Kelemen, Z., Gillikin, D. P., Graniero, L. E., Havel, H., Darchambeau, F., Borges, A. V., et al. (2017). Calibration of hydroclimate proxies in freshwater bivalve shells from Central and West Africa. *Geochimica et Cosmochimica Acta*, *208*, 41–62. https://doi.org/10.1016/j.gca.2017.03.025

Kirchner, J. W. (2006). Getting the right answers for the right reasons: Linking measurements, analyses, and models to advance the science of hydrology. *Water Resources Research*, *42*(3). https://doi.org/10.1029/2005WR004362

Ladson, A. R., Brown, R., Neal, B., & Nathan, R. (2013). A standard approach to baseflow separation using the lyne and hollick filter. *Australasian Journal of Water Resources*, *17*(1), 25–34. https://doi.org/10.7158/13241583.2013.11465417

Laudon, H., Hasselquist, E. M., Peichl, M., Lindgren, K., Sponseller, R., Lidman, F., et al. (2021). Northern landscapes in transition: Evidence, approach and ways forward using the Krycklan catchment study. *Hydrological Processes*, *35*(4), e14170. https://doi.org/10.1002/hyp.14170

Laudon, H., Sjöblom, V., Buffam, I., Seibert, J., & Mörth, M. (2007). The role of catchment scale and landscape characteristics for runoff generation of boreal streams. *Journal of Hydrology*, *344*, 198–209. https://doi.org/10.1016/j.jhydrol.2007.07.010

Lehner, B., Verdin, K., & Jarvis, A. (2008). New global hydrography derived from spaceborne elevation data. *Eos, Transactions American Geophysical Union*, *89*(10), 93–94. https://doi.org/10.1029/2008EO100001

Lindström, G., & Bergström, S. (2004). Runoff trends in Sweden 1807–2002. *Hydrological Sciences Journal*, *49*, 69–83. https://doi.org/10.1623/hysj.49.1.69.54000

Liu, B., Yang, D., Ye, B., & Berezovskaya, S. (2005). Long-term open-water season stream temperature variations and changes over Lena River Basin in Siberia. *Global and Planetary Change*, *48*(1–3), 96–111. https://doi.org/10.1016/j.gloplacha.2004.12.007

Lydeard, C., & Cummings, K. S. (2019). *Freshwater mollusks of the world: A distribution Atlas* (p. 256). JHU Press.

Lyne, V., & Hollick, M. (1979). Stochastic time-variable rainfall-runoff modelling. In *Institute of engineers Australia national conference* (Vol. 79(10), pp. 89–93). Institute of Engineers Australia.

Meriö, L. J., Ala-aho, P., Linjama, J., Hjort, J., Kløve, B., & Marttila, H. (2019). Snow to precipitation ratio controls catchment storage and summer flows in boreal headwater catchments. *Water Resources Research*, *55*(5), 4096–4109. https://doi.org/10.1029/2018WR023031

Mutvei, H., Dunca, E., Timm, H., & Slepukhina, T. (1996). *Structure and growth rates of bivalve shells as indicators of environmental changes and pollution* (Vol. S14–4, pp. 65–72). Bulletin de l'Institut Oceanographique

Mutvei, H., & Westermark, T. (2001). How environmental information can be obtained from naiad shells. In G. Bauer & K. Wächtler (Eds.), *Ecology and evolution of the freshwater Mussels Unionoida, ecological studies* (pp. 367–379). Springer. https://doi.org/10.1007/978-3-642-56869-5_21

Nathan, R. J., & McMahon, T. A. (1990). Evaluation of automated techniques for base flow and recession analyses. *Water Resources Research*, *26*(7), 1465–1473. https://doi.org/10.1029/WR026i007p01465

Nelson, D. B., Basler, D., & Kahmen, A. (2021). Precipitation isotope time series predictions from machine learning applied in Europe. *Proceedings of the National Academy of Sciences of the United States of America*, *118*(26), e2024107118. https://doi.org/10.1073/pnas.2024107118

Ninokawa, A. T., & Ries, J. (2022). Responses of freshwater calcifiers to carbon-dioxide-induced acidification. *Journal of Marine Science and Engineering*, *10*(8), 1068. https://doi.org/10.3390/jmse10081068

Peralta-Tapia, A., Sponseller, R. A., Ågren, A., Tetzlaff, D., Soulsby, C., & Laudon, H. (2015). Scale-dependent groundwater contributions influence patterns of winter baseflow stream chemistry in boreal catchments. *Journal of Geophysical Research: Biogeosciences*, *120*(5), 847–858. https://doi.org/10.1002/2014JG002878

Pfister, L., Grave, C., Beisel, J.-N., & McDonnell, J. J. (2019). A global assessment of freshwater mollusk shell oxygen isotope signatures and their relation to precipitation and streamwater. *Scientific Reports*, *9*(1), 4312. https://doi.org/10.1038/s41598-019-40369-0

Pfister, L., Martínez-Carreras, N., Hissler, C., Klaus, J., Carrer, G. E., Stewart, M. K., & McDonnell, J. J. (2017). Bedrock geology controls on catchment storage, mixing, and release: A comparative analysis of 16 nested catchments. *Hydrological Processes*, *31*, 1828–1845. https://doi.org/10.1002/hyp.11134

Pfister, L., Thielen, F., Deloule, E., Valle, N., Lentzen, E., Grave, C., et al. (2018). Freshwater pearl mussels as a streamwater stable isotope recorder. *Ecohydrology*, *11*(7), e2007. https://doi.org/10.1002/eco.2007

Ploum, S. W., Lyon, S. W., Teuling, A. J., Laudon, H., & van der Velde, Y. (2019). Soil frost effects on streamflow recessions in a subarctic catchment. *Hydrological Processes*, *33*(9), 1304–1316. https://doi.org/10.1002/hyp.13401

Reynolds, D. J., Edge, D. C., & Black, B. A. (2021). RingdateR: A statistical and graphical tool for crossdating. *Dendrochronologia*, *65*, 125797. https://doi.org/10.1016/j.dendro.2020.125797

Rouse, W. R., Douglas, M. S. V., Hecky, R. E., Hershey, A. E., Kling, G. W., Lesack, L., et al. (1997). Effects of climate change on the freshwaters of Arctic and Subarctic North America. *Hydrological Processes*, *11*(8), 873–902. https://doi.org/10.1002/(SICI)1099-1085(19970630)11:8<873::AID-HYP510>3.0.CO;2-6

Schöne, B. R., Dunca, E., Fiebig, J., & Pfeiffer, M. (2005). Mutvei's solution: An ideal agent for resolving microgrowth structures of biogenic carbonates. *Palaeogeography, Palaeoclimatology, Palaeoecology*, *228*(1–2), 149–166. https://doi.org/10.1016/j.palaeo.2005.03.054

Schöne, B. R., Dunca, E., Mutvei, H., & Norlund, U. (2004). A 217-year record of summer air temperature reconstructed from freshwater pearl mussels (*M. margaritifera*, Sweden). *Quaternary Science Reviews*, *23*, 1803–1816. https://doi.org/10.1016/j.quascirev.2004.02.017

Schöne, B. R., Meret, A. E., Baier, S. M., Fiebig, J., Esper, J., McDonnell, J., & Pfister, L. (2020). Freshwater pearl mussels from northern Sweden serve as long-term, high-resolution streamwater isotope recorders. *Hydrology and Earth System Sciences*, *24*(2), 673–696. https://doi.org/10.5194/hess-24-673-2020

Tetzlaff, D., Buttle, J., Carey, S. K., Mcguire, K., Laudon, H., & Soulsby, C. (2015). Tracer-based assessment of flow paths, storage and runoff generation in northern catchments: A review. *Hydrological Processes*, *29*(16), 3475–3490. https://doi.org/10.1002/hyp.10412

Teutschbein, C., Grabs, T., Karlsen, R. H., Laudon, H., & Bishop, K. (2015). Hydrological response to changing climate conditions: Spatial streamflow variability in the boreal region. *Water Resources Research*, *51*(12), 9425–9446. https://doi.org/10.1002/2015WR017337

Teutschbein, C., Grabs, T., Laudon, H., Karlsen, R. H., & Bishop, K. (2018). Simulating streamflow in ungauged basins under a changing climate: The importance of landscape characteristics. *Journal of Hydrology*, *561*, 160–178. https://doi.org/10.1016/j.jhydrol.2018.03.060

Teutschbein, C., Quesada Montano, B., Todorović, A., & Grabs, T. (2022). Streamflow droughts in Sweden: Spatiotemporal patterns emerging from six decades of observations. *Journal of Hydrology: Regional Studies*, *42*, 101171. https://doi.org/10.1016/j.ejrh.2022.101171

Tiwari, T., Buffam, I., Sponseller, R. A., & Laudon, H. (2017). Inferring scale-dependent processes influencing stream water biogeochemistry from headwater to sea. *Limnology & Oceanography*, *62*(S1), S58–S70. https://doi.org/10.1002/lno.10738

Tiwari, T., & Laudon, H. (2025). Trends in hydroclimate extremes: How changes in winter affect water storage and baseflow. *Hydrology and Earth System Sciences*, *29*(17), 4055–4071. https://doi.org/10.5194/hess-29-4055-2025

Tiwari, T., Laudon, H., Beven, K., & Ågren, A. M. (2014). Downstream changes in DOC: Inferring contributions in the face of model uncertainties. *Water Resources Research*, *50*(1), 514–525. https://doi.org/10.1002/2013WR014275

Türk, G., Gey, C. J., Schöne, B. R., & Pfister, L. (2025). Effects of synoptic atmospheric variability on sub-daily precipitation δ^{18}O-air temperature functions in reconstructions of pre-instrumental δ^{18}O chronicles across Europe. *EGUsphere*, 1–26. https://doi.org/10.5194/egusphere-2024-4169

Versteegh, E. A. A., Vonhof, H. B., Troelstra, S. R., Kaandorp, R. J. G., & Kroon, D. (2010). Seasonally resolved growth of freshwater bivalves determined by oxygen and carbon isotope shell chemistry. *Geochemistry, Geophysics, Geosystems*, *11*(8). https://doi.org/10.1029/2009GC002961

Wilson, D., Hisdal, H., & Lawrence, D. (2010). Has streamflow changed in the nordic countries? – Recent trends and comparisons to hydrological projections. *Journal of Hydrology*, *394*(3–4), 334–346. https://doi.org/10.1016/j.jhydrol.2010.09.010

Zhang, X., Harvey, K. D., Hogg, W. D., & Yuzyk, T. R. (2001). Trends in Canadian streamflow. *Water Resources Research*, *37*(4), 987–998. https://doi.org/10.1029/2000WR900357